The Role of Pulsed Electromagnetic Fields on the Radical Pair Mechanism

Pablo Castello,[1] Pablo Jimenez,[2] and Carlos F. Martino[3]*

[1]Consejo Nacional de Investigaciones Científicas y Técnicas (CONICET), Facultad de Ciencias Exactas y Naturales, Universidad de Belgrano, Buenos Aires, Argentina
[2]Centro Atómico Bariloche, CONICET, CNEA, S. C. de Bariloche, Argentina
[3]Johns Hopkins University Applied Physics Laboratory, Laurel, Maryland

In recent decades, the use of pulsed electromagnetic fields (PEMF) in therapeutics has been one of the main fields of activity in the bioelectromagnetics arena. Nevertheless, progress in this area has been hindered by the lack of consensus on a biophysical mechanism of interaction that can satisfactorily explain how low-level, non-thermal electromagnetic fields would be able to sufficiently affect chemistry as to elicit biological effects in living organisms. This specifically applies in cases where the induced electric fields are too small to generate a biological response of any consequence. A growing body of experimental observations that would explain the nature of these effects speaks strongly about the involvement of a theory known as the radical pair mechanism (RPM). This mechanism explains how a pair of reactive oxygen species with distinct chemical fate can be influenced by a low-level external magnetic field through Zeeman and hyperfine interactions. So far, a study of the effects of complex spatiotemporal signals within the context of the RPM has not been performed. Here, we present a computational investigation of such effects by utilizing a generic PEMF test signal and RPM models of different complexity. Surprisingly, our results show how substantially different chemical results can be obtained within ranges that depend on the specific orientation of the PEMF test signal with respect to the background static magnetic field, its waveform, and both of their amplitudes. These results provide a basis for explaining the distinctive biological relevance of PEMF signals on radical pair chemical reactions. © 2021 Bioelectromagnetics Society.

Keywords: **magnetic effects; PEMFs; radical pair mechanism; reactive oxygen species; spin biochemistry**

INTRODUCTION

A significant body of evidence has been amassed for years supporting "non-thermal" biological effects resulting from exposures to low-level magnetic fields [Barnes and Greenebaum, 2018]. When these exposures take place at the cellular level, two components can be observed: a magnetic component and an electric component. Each of these components can be conveniently separated into static and time-varying parts, which are the result of the combination of the actual intended magnetic exposure and background fields that already exist in the environment [Portelli, 2017]. Of these, it is the electrical component (or the induced electric field-IEF) that is where biological effects have traditionally been better demonstrated, understood, and replicated, which resulted in it being today the most established within the scientific community. So, it is mostly within these observed

Grant sponsor: National Science Foundation, grant number: 2051510, 2020.

Conflicts of interest: None.

*Correspondence to: Carlos F. Martino, Johns Hopkins University Applied Physics Laboratory, Laurel, MD 20723.
E-mail: Carlos.Martino@jhuapl.edu

Received for review 22 September 2020; Revised 8 June 2021; Accepted 19 June 2021

DOI:10.1002/bem.22358
Published online 00 Month 2021 in Wiley Online Library (wileyonlinelibrary.com).

biological effects and possible hazards that the fundamental basis for our current safety standards has been constructed, which have persisted with little modifications since their inception [International Commission on Non-Ionizing Radiation Protection, 2002; Matthes et al., 2003; World Health Organization, 2007; International Commission on Non-Ionizing Radiation Protection, 2010; Lagroye, 2020].

Simultaneously, a plethora of evidence has been accumulated on models ranging from cell-free molecular studies to plants and complex animals, showing clear dependence on the orientation and magnitude of the low-level static magnetic field (SMF) component [Markov and Pilla, 1994; Markov and Pilla, 1997; Johnsen and Lohmann, 2005; Mouritsen and Ritz, 2005; Wiltschko and Wiltschko, 2006; Ahmad et al., 2007; Solov'yov et al., 2007; Solov'yov and Greiner, 2007; Binhi and Prato, 2017; Prato and Binhi, 2017; Greenebaum, 2018]. Meticulous researchers have also noted that the role of low-level SMFs in the vicinity of the experimental setup (typically of the order of that found naturally on Earth's surface, i.e., on unperturbed conditions) is sometimes a crucial factor for observing time-varying magnetic field effects [Blackman et al., 1985; Yost and Liburdy, 1992; Markov et al., 1993; Pilla, 2007; Castello et al., 2014; Usselman et al., 2016; Albaqami et al., 2020; Luukkonen et al., 2020]. In fact, some experiments have shown how the static component was able to generate larger effects without (rather than with) the time-varying components tested, even when these magnitudes were close to 0 μT [Walleczek and Liburdy, 1990; Markov et al., 1993; Markov and Pilla, 1997]. Perhaps more interestingly, some reports have been quite emphatic on the fact that the effects observed appear to be strictly dependent on the relative orientation (angle) between the *static* and *time-varying* components, frequently commenting on the fact that effects appear (or disappear) when flux densities are perpendicular from one another (or sometimes, vice versa) [Smith et al., 1987; Yost and Liburdy, 1992]. In the same way, the apparent sensitivity to this factor and its interdependence with the other parameters (amplitude, waveform, time of exposure) of the components has been frequently reported, hinting at the apparent existence of "windows" (both from the physical and biological sense) within which effects may (or may not) be observed [Blackman et al., 1985; Smith et al., 1987; Walleczek and Liburdy, 1990; Markov, 2005].

Of the several potential mechanisms cited, the spin-correlated radical pair mechanism (RPM) offers, in our opinion, the best understood and established explanation of how magnetic fields might influence biochemical reactions [Steiner and Ulrich, 1989; Hore and Mouritsen, 2016]. Magnetic field effects are possible during the singlet-triplet spin evolution of two radicals, which are in proximity, or in the same "cage," that form a radical pair [Steiner and Ulrich, 1989; Solov'yov and Schulten, 2009]. Applied magnetic fields can affect two main internal interactions of the radical pair whose time-dependence affect the temporal evolution of the singlet-triplet mixing, and thereby modulate relative reaction rates [Massey, 1994]: electron-nuclear hyperfine interactions (HFI) and radical Zeeman energies; both interactions have energies much smaller than k_BT thermal energy, which is 0.0259 eV at room temperature. In other words, the RPM is typically an adiabatic process, uncoupled to the thermal bath; therefore, "non-thermal effects" of magnetic fields in biological systems are expected through these magnetic field and resonant frequency regimes without the explicit influence of temperature. An oscillating magnetic field that is in resonance with the splitting between radical pair spin states can perturb radical pair dynamics by driving [Solov'yov and Schulten, 2009] singlet-triplet transitions [Schulten and Wolynes, 1978; Solov'yov and Schulten, 2009] in the region where the exchange interaction $J_{ex}(r)$ is neglected. In typical biological molecules, many hyperfine splittings occur in the range of 0.1–10 MHz [Cintolesi et al., 2003]. The effect of the HFI and Zeeman resonances are dependent on the frequency, magnitude, and orientation of magnetic fields; these parameters can thus, in principle, significantly influence the relative reaction rates and product distributions of reactions of radical pairs.

Several studies support this hypothesis. For example, it was tested by developing an instrumentation for product-yield detected magnetic resonance, where primary human umbilical vein endothelial cells were exposed to either 50 μT SMFs in control samples, or to SMFs combined with 1.4 MHz, 10 μT radiofrequency magnetic fields at Zeeman resonance in experimental samples. The magnetic field orientation was applied in parallel or perpendicular angles with respect to the SMF. Results showed changes in reactive oxygen species (ROS) products in cell cultures as a function of the orientation of SMF and oscillating magnetic field; these are indicative of a resonance effect on the singlet-triplet intersystem crossing at the point of ROS formation. The authors subsequently showed the effects of ROS partitioning on cellular bioenergetics [Usselman et al., 2016].

Although animal and human exposure to complex electromagnetic signals (most interestingly pulsed electromagnetic field [PEMF] signals) is

widespread today, their role has not been studied extensively within the RPM theoretical framework, and the extent to which the observed effects could be due to exclusively the magnetic component of the waveform remains largely unexplored and unknown. In this manuscript, we explore the relevance of simple PEMF test signals on the resulting product yield of some model radical pair reactions as "proof of principle." With this approach, we seek to gain some insight into the degree these signals could later invoke a differential biological response. We achieve this through simulations with simple square waveforms on models with one, two, and five hyperfine constants. This mechanism has been intensively studied before for several model systems [Schulten et al., 1976; Werner et al., 1977; Schulten et al., 1978; Schulten, 1982; Schulten, 1984; Ritz et al., 2000; Rodgers et al., 2007]. In the suggested radical pair scenario, one radical is devoid of HFI [Solov'yov and Schulten, 2009]. We address the possible limitations of this model in the "Discussion" section. Indeed, here we demonstrate how chemical product yields that are modeled by the RPM can be substantially modulated by the relative orientation of a PEMF test signal in relation to a static background magnetic field (which could be of the magnitude of the Earth's magnetic field), and their amplitudes and fundamental frequency in a manner that is analog, but substantially different from a sinusoidal test waveform.

THEORY

In this section, the computational description of the magnetic field dependence in the radical pair reaction is described. We choose to work in the Schrödinger representation for mathematical convenience. We assume that the radical pair is created in the singlet state; subsequent analysis is similar for triplet-born radicals.

Statement of the Problem

We consider computing the singlet quantum yield given by Canfield [1997], Ritz et al. [2000], Solov'yov and Schulten [2009]

$$J(\psi, u) = k_s \int \langle \psi(t, u(t)) | P_S | \psi(t, u(t)) \rangle dt \quad (1)$$

ψ(t) is the wave function, the evolution of which is governed by the time-dependent Schrödinger equation

$$i\frac{\partial \psi(t)}{\partial t} = H(u(t))\psi(t), 0 \le t \le T \quad (2)$$

with initial condition $\psi(0) = \phi_s$, which represents a singlet-born radical. Here, H denotes the spin Hamiltonian of the radical, k_s is the rate constant for the escape process of the radicals, and $u(t)$ is the time-dependent magnetic field, which includes the earth's magnetic field. Planck's constant has been set to 1.

P_S in Equation (1) is the projection operator onto the singlet state of the electron spin pair,

$$P_S = \frac{1}{4}E - S_1 \cdot S_2, \quad (3)$$

where S_1 and S_2 denote the electron spin operators of the radicals, and $\boldsymbol{E}$ is the identity matrix.

Spin Hamiltonian

As explained in the literature [Canfield, 1997; Ritz et al., 2000; Solov'yov and Schulten, 2009], the spin Hamiltonian is composed of Zeeman and hyperfine coupling interactions and can be written for a one-proton model as

$$H(u(t)) = \mu_B g S_1 \cdot u + \mu_B g S_2 \cdot u + \mu_B g I_1 \cdot A_1 \cdot S_1 - \frac{i}{2}(k_s P_S + k_t P_T) \quad (4)$$

where P_T is the triplet projection operator defined by $P_T + P_S = 1$, $I_1 = (I_{1x}, I_{1y}, I_{1z})$ is the spin operator of nucleus 1, and $S_{1,2} = (S_x, S_y, S_z)$ are the electron's spin operators defined as

$$S_1 = \left(\frac{1}{2}\sigma_x \otimes E_2 \otimes E_2, \frac{1}{2}\sigma_y \otimes E_2 \otimes E_2, \frac{1}{2}\sigma_z \otimes E_2 \otimes E_2\right), S_2 = \left(E_2 \otimes \frac{1}{2}\sigma_x \otimes E_2, E_2 \otimes \frac{1}{2}\sigma_y \otimes E_2, E_2 \otimes \frac{1}{2}\sigma_z \otimes E_2\right) \quad (5)$$

where $(\sigma_x, \sigma_y, \sigma_z)$ are Pauli's spin matrices acting on the electron's spins, $(\cdot,\cdot)$ denotes inner product, and E_2 is the 2×2 identity matrix. The symbol $\otimes$ denotes tensor product between appropriate Hilbert Spaces. The last term is the Haberkorn term "K" in an effective non-Hermitian Hamiltonian. This includes the effects of singlet and triplet radical pairs reacting at different rates k_s, k_t, respectively. The components (x,y,z) represent the Cartesian components of the geometrical space.

In Equation (4), $A_1 = (A_x, A_y, A_z)$ is the hyperfine tensor for nucleus 1, usually anisotropic, μ_B is the Bohr magneton, and $u(t)$ is the external magnetic field, the control function.

The Spin Hamiltonian for a one-proton model can be further simplified to

$$\begin{aligned} H = {} & \mu_B g(S_{1x} + S_{2x})u_x + \mu_B g(S_{1y} + S_{2y})u_y \\ & + \mu_B g(S_{1z} + S_{2z})u_z + \mu_B g I_{1x} A_{1x} S_{1x} \\ & + \mu_B g I_{1y} A_{1y} S_{1y} + \mu_B g I_{1z} A_{1z} S_{1z} \\ & - \frac{i}{2}(k_s P_S + k_t P_T) \end{aligned} \tag{6}$$

We emphasize that the external magnetic field $u(t)$ can be an arbitrary input function.

Numerical Approach

We performed a Python-based program to solve Schrödinger's equation and calculate the quantum yield numerically for 1, 2, and 5 proton model. This equation is a linear homogeneous Ordinary Differential Equation, which can be written as the following:

$$\frac{\partial \psi}{\partial t} - iH(t)\psi = 0$$

For this equation, we can obtain the wave function $\psi(t)$ by applying many times the short time evolution operator

$$\psi(t + \Delta) = U(t)\psi(t),\ U(t) = e^{-i\int_t^{t+\Delta} H dt}$$

We establish a time step $\Delta = 7\,\text{ns}$ and evolve the wave function 2,000 times from 0 to 14 μs.

Once this equation is solved, we calculate numerically the quantum yield by using numerical integral methods.

RESULTS

We present some illustrative examples of a model radical pair to demonstrate the differential effects of PEMF test signals in a radical pair reaction as a function of intensity and orientation with respect to a background SMF. We consider models with one, two, and five hyperfine constants. We begin with one spin $\frac{1}{2}$ nucleus, whose anisotropic constants are $a_{1x} = -0.234$, $a_{1y} = -0.234$, $a_{1z} = 0.117$ all in mT [Cintolesi et al., 2003]. The PEMF test signal consists of a square waveform with varying fundamental frequencies and is implemented perpendicular to a background magnetic field of the order of the static component of the naturally occurring Earth's magnetic field. Subsequent examples will indicate the magnitude and direction on the PEMF test signal relative to the background, as well as the hyperfine parameters for higher-dimensional cases.

The One-Proton Radical Pair

Validation of the model. To illustrate the use of Equations (1) and (2), and to start our discussion, we validate the model with the case of a radical pair with a single spin-$\frac{1}{2}$ nucleus and a sinusoidal waveform magnetic field ranging on frequency from $0 \leq \omega \leq 10$ MHz, $u(t) = u_0 \sin(\omega t)$. We note that the model must be validated in each case as the singlet yield baseline will change as hyperfine parameters are added. Here u_0 and $\frac{1}{k_s}$ are 2 μT and 2 μs, respectively. The configuration of the magnetic fields are as follows: the background SMF of 50 μT (as a representation within the magnitude range found in the northern hemisphere [Finlay et al., 2010]) is applied in the z direction; the sinusoidal waveform $u(t)$ is applied in the x direction. The spin Hamiltonian simplifies to

$$\begin{aligned} H = {} & \mu_B g(S_{1x} + S_{2x})u_x + \mu_B g(S_{1z} + S_{2z})b_0 + \mu_B g I_1 \\ & \cdot A_1 \cdot S_1 - \frac{i}{2}(k_s P_S + k_t P_T) \end{aligned} \tag{7}$$

where b_0 is the background SMF, u_x is the x component of the sinusoidal waveform, and I_1, S_1, and S_2 are the spin angular momentum operators of the nucleus and two electrons. Figure 1 shows the effect of this validation on the singlet quantum yield of a one-proton radical pair, calculated using Equation (1), for various frequency ranges. The abrupt drop in J produced at 1.4 MHz is the result of one of the radicals being devoid of HFI. Other small resonances are due to interaction with hyperfine constants.

Low-intensity PEMFs applied perpendicular to a background static field decreases singlet yield. Now that the model produces similar results to that stated in the literature for a one-proton model [Ritz et al., 2000], we proceed next with a similar configuration introducing a square waveform with a varying fundamental frequency as the PEMF test signal (nature of biphasic waveform is not important here). The initial input (not shown) is just a constant field (zero frequency) at 2 μT intensity. The test

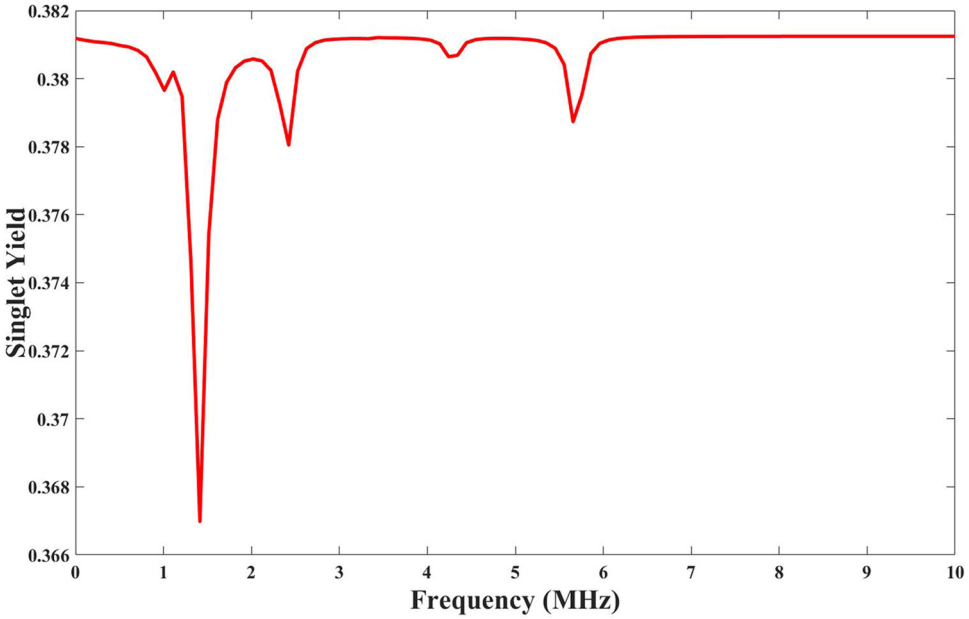

Fig. 1. Singlet product yield for a one-proton model. Sinusoidal test signal (2 μT peak) is applied perpendicularly to a background static field (50 μT).

signals vary in frequency by up to 200 different frequency data points. The rationale to introduce a train of pulses that vary in frequency, i.e., one long pulse up to eight pulses (Fig. 2a), is not to study the frequency response of the system, but rather to have a continuous set of yields for comparison. Singlet yield in Equation (1) is computed at each step. In particular, for the waveform with 7 pulses, which corresponds to a frequency of 500 KHz, Equation (1) provides a single point for the quantum yield for the singlet product of 0.3812 (Fig. 2c). Figure 2a shows ten signals; the last PEMF test signal (500 kHz) is shown in Figure 2b. For an SMF and very low-frequency pulse, the singlet product yield of 0.3812 is very close to the case where the background SMF is that mimicking Earth's (50 μT), Figure 2c. A significant result is a decrease in singlet product yield as the frequency increases with PEMF test signal increases. This is reminiscent of the abrupt drop of singlet product yield for an oscillating magnetic field at the Zeeman frequency (Fig. 1).

Singlet product yield responds to PEMFs' relative orientation to the background static field. We increase the amplitude of the square waveform test signal to (±) 200 μT, a typical amplitude found in PEMF literature. The test signal is the same as in Figure 2 (now implemented in perpendicular and parallel orientation to the background static field). Here, the singlet yield increases to 0.43 (by ~13%) when the test signal is constant (Fig. 3). As the frequency of the PEMF test signal increases, the singlet product yield decreases slowly to a minimum of 0.32 while several "windows" are observed. The same PEMF test signal is implemented in parallel to the SMF (z direction) in Figure 3. For this case, we observe a slight increase in the static and low-frequency pulse portion of the singlet product yield as compared with the static and low-intensity case, with "windows" that appear at other frequencies. Interestingly, at higher frequencies, we can also observe the "windows" for which the singlet product yield is reversed (Fig. 3). Therefore, for the same frequency range, we observe that while for the perpendicular case the singlet product yield can decrease by up to ~34%, in the parallel case it could increase by up to ~17% (both compared to their static case).

PEMF Effects on the Two-Proton Radical Pair

The results above may be extended readily to radicals bearing two hyperfine constants. We proceed to validate the two-proton model with the following hyperfine parameters: $a_{1x} = -0.234$, $a_{1y} = -0.234$, $a_{1z} = 0.117$, $a_{2x} = -0.03$, $a_{2y} = -0.022$, $a_{2z} = 0.688$ all in mT [Cintolesi et al., 2003] (see Fig. 4a). The Zeeman resonance at 1.4 MHz is expected, as one of the radicals is devoid of HFI. Then, we compute the singlet product yield only for the same PEMF test signal described in the previous examples in perpendicular and in parallel (Fig. 4b) to the same

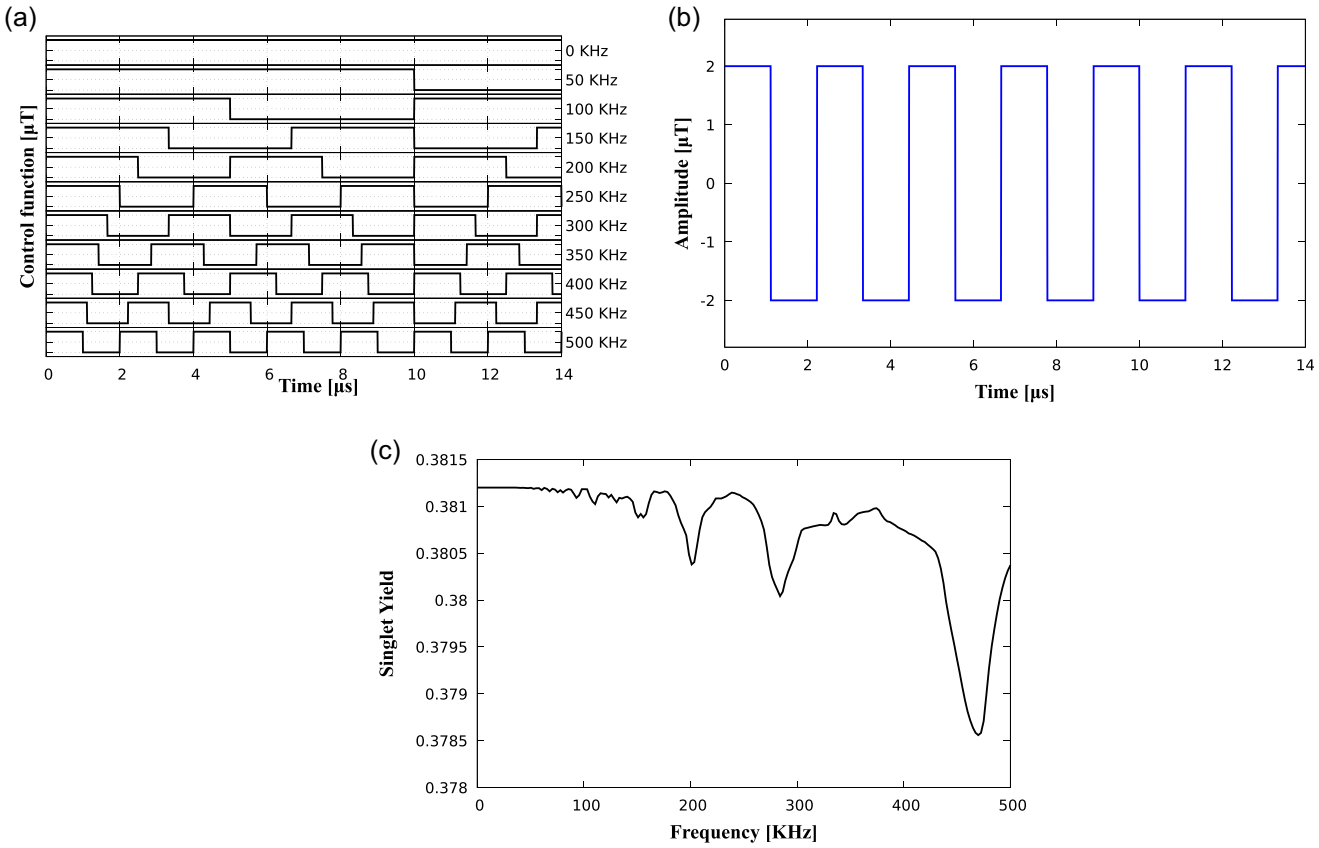

Fig. 2. Singlet product yield for a one-proton model implemented in perpendicular to a background static field (50 μT). (**a**) Test signal: Square waveform (PEMF) of ±2 μT varying in frequency. (**b**) Last pulse is shown. (**c**) Singlet product yield decreases significantly for the same frequency band as the PEMF test signal is used. PEMF = pulsed electromagnetic field.

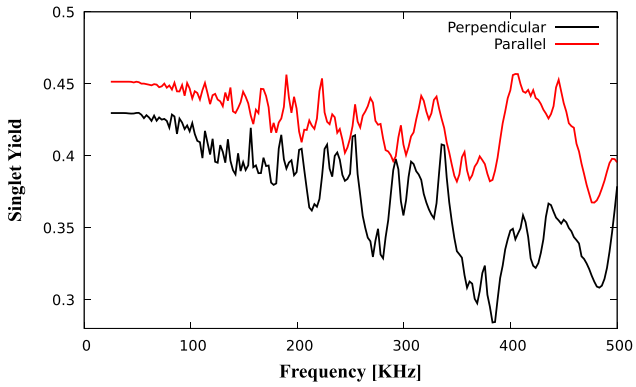

Fig. 3. Singlet product yield as a function of relative orientation of a square waveform (PEMF) at ±200 μT test signal and a static background field (50 μT) for a one-proton model (as in Fig. 2). (**a**) Test signal is implemented in perpendicular to background static field. (**b**) Test signal is implemented in parallel to the background static field. PEMF = pulsed electromagnetic field.

background static field. The differential effects in product yield (modulation into "windows" at higher frequencies) as a function of the relative orientation of the PEMF test signal for the two-proton model are clear.

PEMF Effects on More Complex Radical Pairs

The isotropic hyperfine coupling constants and the principal values of the hyperfine tensor used in these calculations are given in Table 1. The data were obtained by this paper [Cintolesi et al., 2003]. The product yield for the five-spin-$\frac{1}{2}$ nuclei is shown in Figure 5a. It is evident from Figure 5b that while the singlet product yield differences are smaller than for the other models, they are a function of orientation, and the decrease in product yield is significantly greater for the perpendicular orientation.

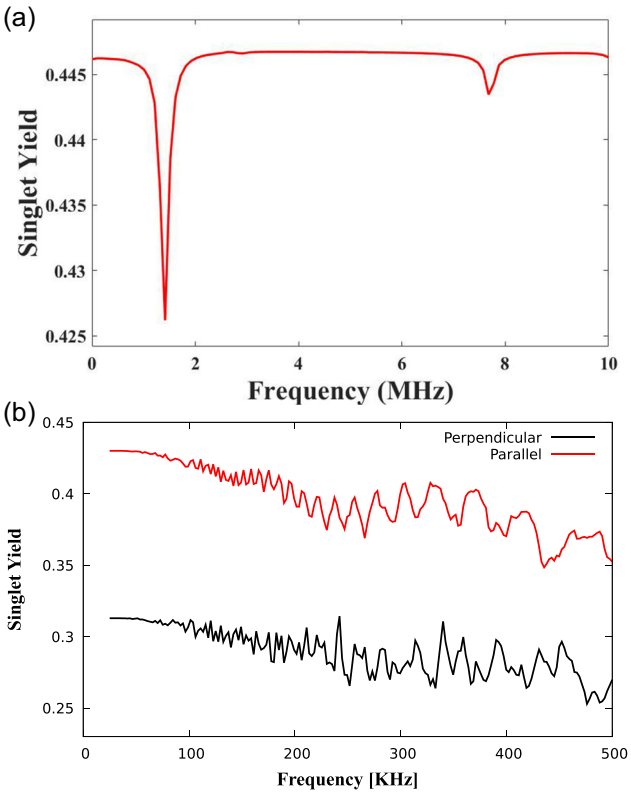

Fig. 4. Singlet product yield as a function of relative orientation of the square waveform (PEMF) at ±200 μT test signal and the static background field (50 μT) for a two-proton model (as in Fig. 2). (**a**) Validation of the model with a sinusoidal test signal (2 μT peak) applied perpendicularly to a background static field (50 μT). (**b**) Test signal is implemented in perpendicular and in parallel to background static field. PEMF = pulsed electromagnetic field.

TABLE 1. Isotropic Hyperfine Coupling Constants (a_{iso}), Principal Values of the Anisotropic Part of the Hyperfine Tensors for Nuclei in the Neutral Flavin Radicals [Cintolesi et al., 2003]

Radical	Nucleus	a_{iso}	T_{ii}
FH	N5	0.393	−0.498
			−0.492
			0.989
	N10	0.212	−0.242
			−0.234
			0.476
	H1r	0.390	−0.062
			−0.033
			0.095
	H6	−0.158	−0.060
			−0.044
			0.104
	H5	−0.769	−0.616
			−0.168
			0.784

Units are in mT.

DISCUSSION

In this pilot exploration, we describe the extent to which square waveforms may affect radical pair reaction product yields by focusing our attention on the magnitude and orientation of our PEMF test signal for a singlet-born radical pair. The present study does not consider variations in yield as a result of changes in phase between input waveform and radical pair formation. The singlet product yields for the one-nucleus radical pair depicted in Figure 2c show a variety of effects for this simple model. Product yield decreases significantly with the fundamental frequency of the PEMF test signal implemented in perpendicular to the static background field at low magnitude when compared with the sinusoidal waveform used for validation of the model (Fig. 1). Our second example on the same model at higher amplitude (Fig. 3) shows not only how the product yield is substantially dependent on the amplitude of the PEMF test signal, but also on its alignment with respect to the static background field (a hallmark of RPM). Interestingly, frequency regions within these examples where differential effects can be observed subject to orientation become clear. Differential effects depending on the orientation of the PEMF test signal and the background static field are also observed for a two-proton model. Once again, the hallmark of RPM is repeated here. The true test for the radical pair model comes with more complex five-proton nuclei. In this example, the singlet yield for the validation sinusoidal waveform decreases slightly at the Zeeman frequency; see Figure 5a. In this model, both PEMF test signals in perpendicular or parallel to static background field lead to decreases in the singlet quantum yield. The applied perpendicular PEMF test signal leads to a minimum more efficiently; see Figure 5b.

The RPM model applied to PEMF presented here provides such a framework that not only needs to be investigated deeply but also already points to necessary experiments to be performed to test the rationale. In this regard, any theoretical work is not without limitations. One of the assumptions made here is that one radical is devoid of HFI; clearly, this is an open question that would still have to be verified experimentally. Such a radical, for example, could be superoxide. Superoxide is devoid of HFI, which theoretically enters the Hamiltonian and provides specific effects, such as resonance at 1.4 MHz. So far, the involvement of superoxide has been corroborated only indirectly. We note that

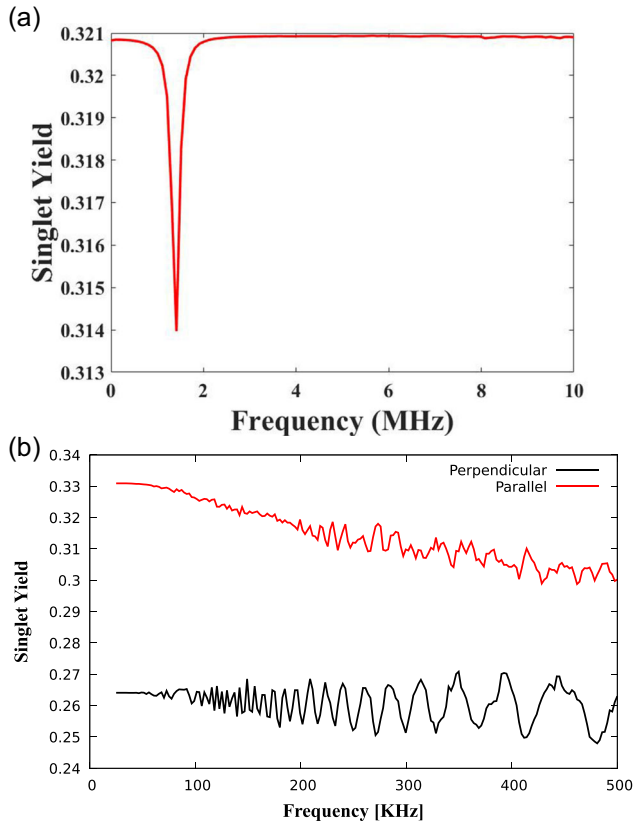

Fig. 5. Singlet product yield as a function of relative orientation of the square waveform (PEMF) at ±200 μT test signal and the static background field (50 μT) for a five-proton model (as in Fig. 2). (**a**) Validation of the model with a sinusoidal test signal (2 μT peak) applied perpendicularly to a background static field (50 μT). (**b**) Test signal is implemented in perpendicular and in parallel to the background static field. PEMF = pulsed electromagnetic field.

many reports suggest that superoxide is incompatible with magnetic field effects in weak fields as it undergoes rapid spin relaxation that would alleviate the kinds of effects discussed here [Hogben et al., 2009; Karogodina et al., 2011; Kattnig, 2017]. However, a recent study has determined the conditions under which spin relaxation might be slow enough to make superoxide a viable component of the radical pair [Player and Hore, 2019]. These conditions have not been proven nor disproven experimentally. It is beyond the scope of this manuscript to tackle these uncertainties.

It is also tempting to hypothesize that the characteristic "on-off" waveform of a PEMF signal may be part of an optimal set of controls. Although it is difficult to generalize on the basis of a simple model, one may speculate that the so-called "bang-bang" controls may be part of an optimal set that minimizes the singlet quantum yield in Equation (1) in an efficient or perhaps more robust manner as compared with the "classical" sinusoidal waveforms. Exploration of this possibility will be the focus of further work.

CONCLUSION

Experimental observations speak strongly for the involvement of the radical pair mechanism in biological systems. For this purpose, we computationally studied whether a pulse train waveform can change the quantum singlet yields in a radical pair reaction. For a simple radical pair model, we demonstrated that the suggested reaction can be influenced by PEMFs.

This conclusion does not rule out the possibility of induced electric field effects stemming from PEMFs. However, experimental evidence suggests controversial results with the use of PEMFs that cannot be explained by the accepted mechanism of action [Barnes and Greenebaum, 2018]. Our study establishes the role of PEMF as a diagnostic tool that may indicate the involvement of magneto-sensitive radical pair reactions in biological systems. Extending this tool to determine orientation and amplitude dependence in which the input PEMF waveforms affect the reaction products can reveal the chemical nature of the radical pairs involved. Finally, using the oscillating or PEMF input waveform as a diagnostic tool to modify singlet quantum yields can easily be transferred to finding the optimal control to maximize the singlet yield. At the most fundamental level, one could investigate how a radical reaction can be controlled by perturbing spin interconversion to maximize a cost functional, the quantum singlet yield, through the selection of optimal control functions, namely the magnetic waveform.

ACKNOWLEDGMENT

This work was supported by the National Science Foundation Grant Number 2051510, 2020 monitored by Carlos F Martino.

REFERENCES

Ahmad M, Galland P, Ritz T, Wiltschko R, Wiltschko W. 2007. Magnetic intensity affects cryptochrome-dependent responses in Arabidopsis thaliana. Planta 225:615–624.

Albaqami M, Hammad M, Pooam M, Procopio M, Sameti M, Ritz T, Ahmad M, Martino CF. 2020. Arabidopsis cryptochrome is responsive to radiofrequency (RF) electromagnetic fields. Sci Rep 10:1–8.

Barnes FS, Greenebaum B. 2018. Handbook of Biological Effects of Electromagnetic Fields-Two Volume Set. Boca Raton, FL: CRC press. pp. 115–156.

Binhi VN, Prato FS. 2017. Biological effects of the hypomagnetic field: An analytical review of experiments and theories. PLOS One 12:e0179340.

Blackman C, Benane S, Rabinowitz J, House D, Joines W. 1985. A role for the magnetic field in the radiation-induced efflux of calcium ions from brain tissue in vitro. Bioelectromagnetics 6:327–337.

Canfield JM. 1997. Approaching magnetic field effects in biology using the radical pair mechanism [Thesis (PhD)]. p. 4898.

Castello PR, Hill I, Sivo F, Portelli L, Barnes F, Usselman R, Martino CF. 2014. Inhibition of cellular proliferation and enhancement of hydrogen peroxide production in fibrosarcoma cell line by weak radio frequency magnetic fields. Bioelectromagnetics 35:598–602.

Cintolesi F, Ritz T, Kay C, Timmel C, Hore P. 2003. Anisotropic recombination of an immobilized photoinduced radical pair in a 50-μT magnetic field: A model avian photomagnetoreceptor. Chem Phys 294:385–399.

Finlay CC, Maus S, Beggan C, Bondar T, Chambodut A, Chernova T, Chulliat A, Golovkov V, Hamilton B, Hamoudi M. 2010. International geomagnetic reference field: The eleventh generation. Geophys J Int 183:1216–1230.

Greenebaum B. 2018. Mechanisms of action in bioelectromagnetics. In: Barnes FS, Greenebaum B, editors, Bioengineering and Biophysical Aspects of Electromagnetic Fields, Fourth Edition. Boca Raton, FL: CRC Press. pp 233–260.

Hogben HJ, Efimova O, Wagner-Rundell N, Timmel CR, Hore PJ. 2009. Possible involvement of superoxide and dioxygen with cryptochrome in avian magnetoreception: Origin of Zeeman resonances observed by in vivo EPR spectroscopy. Chem Phys Lett 480:118–122.

Hore PJ, Mouritsen H. 2016. The radical-pair mechanism of magnetoreception. Annu Rev Biophys 45:299–344.

International Commission on Non-Ionizing Radiation Protection. 2002. General approach to protection against non-ionizing radiation. Health Phys 82:540–548.

International Commission on Non-Ionizing Radiation Protection. 2010. Guidelines for limiting exposure to time-varying electric and magnetic fields (1 Hz to 100 kHz). Health Phys 99:818–836.

Johnsen S, Lohmann KJ. 2005. The physics and neurobiology of magnetoreception. Nat Rev Neurosci 6:703–712.

Karogodina TY, Dranov IG, Sergeeva SV, Stass DV, Steiner UE. 2011. Kinetic magnetic-field effect involving the small biologically relevant inorganic radicals NO and O2(.-). Chem Phys Phys Chem 12:1714–1728.

Kattnig DR. 2017. Radical-pair-based magnetoreception amplified by radical scavenging: Resilience to spin relaxation. J Phys Chem B 121:10215–10227.

Lagroye I. 2020. International Commission on Non-Ionizing Radiation Protection (ICNIRP): Gaps in knowledge relevant to the "Guidelines for limiting exposure to time-varying electric and magnetic fields (1 Hz–100 kHz)". Health Phys 118:533–542.

Luukkonen J, Naarala J, Juutilainen J, Barnes F, Martino CF. 2020. Pilot study on the therapeutic potential of radiofrequency magnetic fields: growth inhibition of implanted tumours in mice. Br J Cancer 123:1–3.

Markov M, Pilla A. 1994. Static magnetic field modulation of myosin phosphorylation: Calcium dependence in two enzyme preparations. Bioeletrochem Bioenerg 35:57–61.

Markov M, Pilla A. 1997. Weak static magnetic field modulation of myosin phosphorylation in a cell-free preparation: Calcium dependence. Bioeletrochem Bioenerg 43:233–238.

Markov M, Wang S, Pilla A. 1993. Effects of weak low frequency sinusoidal and DC magnetic fields on myosin phosphorylation in a cell-free preparation. Bioeletrochem Bioenerg 30:119–125.

Markov MS. 2005. "Biological windows": A tribute to W. Ross Adey. Environmentalist 25:67–74.

Massey V. 1994. Activation of molecular oxygen by flavins and flavoproteins. J Biol Chem 269:22459–22462.

Matthes R, Vecchia P, McKinlay AF, Veyret B, Bernhardt JH. 2003. Exposure to static and low frequency electromagnetic fields, biological effects and health consequences (0-100 kHz). Review of the scientific evidence on dosimetry, biological effects, epidemiological observations and health consequences concerning exposure to static and low frequency electromagnetic fields (0-100 kHz), ICNIRP 13/2003.

Mouritsen H, Ritz T. 2005. Magnetoreception and its use in bird navigation. Curr Opin Neurobiol 15:406–414.

Pilla AA. 2007. Mechanisms and therapeutic applications of time-varying and static magnetic fields. In: Barnes FS, Greenebaum B, editors, Biological and Medical Aspects of Electromagnetic Fields, Third Edition. Boca Raton, FL: CRC Press. pp 351–412.

Player TC, Hore PJ. 2019. Viability of superoxide-containing radical pairs as magnetoreceptors. J Chem Phys 151:225101.

Portelli L. 2017. Uncertainty Sources Associated With Low-frequency Electric and Magnetic Field Experiments on Cell Cultures. Dosimetry in Bioelectromagnetics. Boca Raton, FL: CRC Press. pp 31–67.

Prato FS, Binhi VN. 2017. Response to comments by Frank Barnes and Ben Greenebaum on" A physical mechanism of magnetoreception: Extension and analysis". Bioelectromagnetics 38:324–325.

Ritz T, Adem S, Schulten K. 2000. A model for photoreceptor-based magnetoreception in birds. Biophys J 78:707–718.

Rodgers CT, Norman SA, Henbest KB, Timmel CR, Hore P. 2007. Determination of radical re-encounter probability distributions from magnetic field effects on reaction yields. J Am Chem Soc 129:6746–6755.

Schulten K. 1982. Magnetic Field Effects in Chemistry and Biology. Festkörperprobleme 22. Berlin, Heidelberg: Springer. pp 61–83.

Schulten K. 1984. Ensemble averaged spin pair dynamics of doublet and triplet molecules. J Chem Phys 80:3668–3679.

Schulten K, Staerk H, Weller A, Werner H-J, Nickel B. 1976. Magnetic field dependence of the geminate recombination of radical ion pairs in polar solvents. Zeitschrift für Physikalische Chemie 101(1–6):371–390.

Schulten K, Swenberg CE, Weller A. 1978. A biomagnetic sensory mechanism based on magnetic field modulated coherent electron spin motion. Z Phys Chem 111:1–5.

Schulten K, Wolynes PG. 1978. Semiclassical description of electron spin motion in radicals including the effect of electron hopping. J Chem Phys 68: 3292–3297.

Smith SD, McLeod BR, Liboff AR, Cooksey K. 1987. Calcium cyclotron resonance and diatom mobility. Bioelectromagnetics 8:215–227.

Solov'yov IA, Chandler DE, Schulten K. 2007. Magnetic field effects in Arabidopsis thaliana cryptochrome-1. Biophys J 92:2711–2726.

Solov'yov IA, Greiner W. 2007. Theoretical analysis of an iron mineral-based magnetoreceptor model in birds. Biophys J 93:1493–1509.

Solov'yov IA, Schulten K. 2009. Magnetoreception through cryptochrome may involve superoxide. Biophys J 96:4804–4813.

Steiner UE, Ulrich T. 1989. Magnetic field effects in chemical kinetics and related phenomena. Chem Rev 89:51–147.

Usselman RJ, Chavarriaga C, Castello PR, Procopio M, Ritz T, Dratz EA, Singel DJ, Martino CF. 2016. The quantum biology of reactive oxygen species partitioning impacts cellular bioenergetics. Sci Rep 6:38543.

Walleczek J, Liburdy RP. 1990. Nonthermal 60 Hz sinusoidal magnetic-field exposure enhances 45Ca2+ uptake in rat thymocytes: Dependence on mitogen activation. FEBS Lett 271:157–160.

Werner HJ, Schulten Z, Schulten K. 1977. Theory of the magnetic field modulated geminate recombination of radical ion pairs in polar solvents: Application to the pyrene–N, N-dimethylaniline system. J Chem Phys 67:646–663.

Wiltschko R, Wiltschko W. 2006. Magnetoreception. BioEssays 28:157–168.

World Health Organization. 2007. Environmental health criteria 238—Extremely low frequency fields. Geneva.

Yost M, Liburdy R. 1992. Time-varying and static magnetic fields act in combination to alter calcium signal transduction in the lymphocyte. FEBS Lett 296:117–122.